Photoactivation of millimeters thick liquid crystal elastomers with broadband visible light using donor-acceptor Stenhouse adducts

*Jesus Guillen Campos,‡ Cassidy Tobin,† Sara Sandlass,† Minwook Park,‡ Yuhang Wu,‡ Michael Gordon,† and Javier Read de Alaniz‡,**

‡ Department of Chemistry and Biochemistry, University of California, Santa Barbara. Santa Barbara, California 93106, United States.
E-mail: javier@chem.ucsb.edu

† Department of Chemical Engineering, University of California, Santa Barbara. Santa Barbara, California 93106, United States.

Keywords: Donor-acceptor Stenhouse adducts, liquid crystal elastomers, photoswitches, visible light actuation, photo-mechanical response.

Abstract

Light-responsive liquid crystal elastomers (LCEs) are stimuli-responsive materials that facilitate the conversion of light energy into a mechanical response. In this work, a novel polysiloxane-based LCE with donor-acceptor Stenhouse adduct (DASA) side-chains was synthesized using a late-stage functionalization strategy. We demonstrate that this approach does not compromise the molecular alignment observed in the traditional Finkelmann method. This easy, single-batch process provides a robust platform to access well-aligned, light-responsive LCE films with thickness ranging from 400 μm to a fourteen-layer stack that is 5 mm thick. Upon irradiation with low-intensity broadband visible light (100 to 200 mW cm^{-2}), these systems undergo 2D planar actuation and complete bleaching. Conversely, exposure to higher-intensity visible light induces bending followed by contraction (300 mW cm^{-2}). These processes are repeatable over several cycles. Finally, we demonstrate how light intensity and the resulting heat generation influences the photothermal stationary state equilibrium of DASA, thereby controlling its photoresponsive properties. This work establishes the groundwork for advancement of LCE-based actuators beyond thin film and UV-light reliant systems.

1. Introduction

Liquid crystal elastomers (LCEs) represent a class of polymer networks with flexible, loosely crosslinking structure and the ability to program molecular orientational order during fabrication. [1–5]A variety of methods including stretching,[6] surface alignment,[7] additive manufacturing,[8] magnetic alignment,[9] and optical pattering[10] can be used to configure the rod-shaped liquid crystal monomers prior to complete polymer network formation. Upon exposure to a stimulus, typically heat or light, the LCE undergoes a reversible structural transition between ordered and disordered states, resulting in macroscopic contraction along the molecular alignment axis (or axes). The permanent crosslinks force molecular order in the network (in most cases a nematic phase) and facilitate reversibility to their initial geometry. Moreover, their elastomeric nature allows for large reversible deformations and shape changes, making them promising candidates for applications in soft robotics,[11–14] nanotechnology,[15–18] and biomimetic materials.[19–22]

The capability to transfer these properties to light-controlled LCEs enables remote control with precise spatial and temporal resolution.[23,24] Photo-responsive molecules incorporated into LCEs can be divided into two main groups: photothermal agents[25] and photoswitches. Photothermal agents can convert the absorbed light into heat through nonradiative relaxation processes. The remotely triggered local temperature increase can cause a phase transition within the LCE, resulting in a macroscopic shape change. However, applying photothermal heat to induce a pre-programmed phase transition is restricted by the constraints of heat transfer, thereby limiting actuation in certain applications (e.g., underwater) or requiring high intensity light (> 0.5 W cm^{-2}) to generate a sufficient temperature increase. Over the past decade, many different types of photothermal agents have been reported to drive LCE phase transitions, including gold metal nanoparticles,[26–28] carbon-based materials,[12,29] and organic dyes.[30,31] The freedom to select from a broad range of photothermal agents has enabled photoresponsive applications using narrowband visible to near-IR light, as well as broadband visible light (i.e., white light). Such use of visible light has a number of advantages that make it an attractive choice for light responsive materials used for biological and material applications. This is in contrast to UV light responsive systems, which

can be harmful to living organisms, have limited penetration depth in materials, and can cause degradation in certain materials upon prolonged exposure.

Controlling LCEs with long wavelength light in the visible to near-IR region poses a major challenge in methods relying on photoswitches to drive the phase transition.[32,33] Moreover, utilizing broadband visible light (380-700 nm) presents particular challenges by impeding the selective excitation of individual photoisomers of the photoswitch.[34,35] In most reports to date, LCEs containing molecular photoswitches have relied on azobenzene, which often require UV light irradiation to trigger *trans-cis* isomerization. The widespread use of azobenzene is likely attributed to availability and the large geometrical change of the *trans*-to-*cis* isomerization that disrupts liquid crystallinity and effectively drives an order to disorder phase transition. Azobenzene's robust chemical structure also facilitates its direct incorporation into various LCE fabrication methods, which, along with its commercial availability, plays a prominent role in its widespread use. However, due to the overlapping absorbance bands of the *trans* and *cis* isomers and use of UV light, most incident photons are absorbed only at the surface within a thickness of less than ≈1-10 μm.[36,37] To improve light penetration and material compatibility, recent investigations have focused on derivatives of azobenzene (e.g., *ortho*-fluorinated azobenzene[38–41] and azotolane[42]**)** known to shift the absorbance of the thermodynamically stable *trans* conformation into the visible spectrum.[34] Red-light controllable systems have also been achieved using azobenzene adducts in combination with upconversion[43] or triplet-triplet annihilation mechanisms.[44] Despite these advancements, efficiently controlling the transition between ordered and disordered states upon irradiation with either UV or visible light in LCEs with thicknesses greater than ≈50 μm has not been achieved using azobenzene-based photochromes. This presents a significant constraint since thin films are more fragile and consequently yield lower overall work output, rendering them less viable for actuating materials.

To truly enable photoisomerization throughout the entire thickness of the sample, negative photochromic properties (i.e., going from colored to transparent form upon photoisomerization) are desired. Aprahamian, Katsonis and co-workers demonstrated this property in shape-persistent LCE

actuators bearing a hydrozone photoswitch.[45] Irradiation with 405 nm light (blue light) causes the polymer ribbon to bend toward the light, and as irradiation proceeds, the ribbon bends back to its original shape. It is believed this occurs as a result of isomerization proceeding throughout the entire sample and achieving a uniform photostationary state. However, the thickness of the LCE used for this study was only 25 μm and 365 nm light is required for the reverse photoisomerization. Negative photochromic properties of diarylethene (DAE)-based LCEs have also recently been used for developing logic AND gate systems with macroscopic output; deformation is negligible when exposed only to UV or visible irradiation, but photothermal driven shape changes are observed when exposed to both simultaneously.[46] Furthermore, White and Bowman have also described the photomechanical actuation of DAE-containing LCEs,[47] resulting in a strain of 5.5%. The light-induced deformation of these materials occurs via the photoisomerization of the DAE, transitioning from the open-ring to the closed-ring structure with UV light, while narrowband visible light (525 nm, 50 mW cm^{-2}) was used to restore the original shape. Nevertheless, a challenge encountered with all the aforementioned photoswitch-driven light-responsive LCEs is the use of thin films (average 10-50 μm), reliance on UV light for either the forward or reverse reaction, and/or limited light-penetration depth. In addition, compared to the available chemical space of photoswitchable motifs – such as azoheteroarenes, diazocines, spiropyran (SP), arylhyrazones, diarylethane (DAE), donor-acceptor Stenhouse adducts (DASA), fulgides, indigoid, hemiindigo, dihydropyrene (DHP), stiff-stilbene, and many more[48] – their use in light-responsive LCEs remains largely unexplored. Use of photoswitches that facilitate the use of visible to near-IR light and allow complete light penetration through thick LCE films will pave the way for future applications at the intersection of soft robots and biological organisms.

Herein, we introduce a photoswitching molecule capable of reversible photoisomerization across the entire thickness of aligned LCEs, ranging from 400 μm to 5 mm. To achieve this, we developed a novel late-stage functionalization strategy, compatible with the original Finkelmann method, for incorporating donor-acceptor Stenhouse adducts (DASA) into siloxane-based LCEs. Significantly, this new method facilitates the incorporation of DASA, which is traditionally incompatible with LCE

synthesis, and enables the fabrication of thick aligned films (**Figure 1**).[49] Among available visible light responsive photoswitches, DASAs stand out owing to their synthetic accessibility, negative photochromic properties and multi-stage switching.[50] DASA photoisomerization involves a reversible transition from a stable linear (open), highly conjugated, colored isomer to a thermally metastable closed (cyclic), colorless state upon irradiation with visible light. This process is classified as negative photochromism, and herein this reversible switching is referred to as *bleaching*.[50–53] The multi-step isomerization enables complex switching phenomena and the ability to tune the population of intermediates along the multi-step reaction pathway of the DASAs without interfering with either the first or final stages.[54] For applications requiring broadband visible light, the spectral properties of DASA are advantageous, since the absorbance of the open and closed isomers do not overlap in the visible region. This enables selective excitation of the open form with broadband visible light (380-700 nm, white light). The negative photochromic properties and ability to use white light is advantageous for bulk solid-state applications,[55] facilitating control over the spatial distribution of colored and colorless forms,[56] thereby enabling tunability in the depth of light penetration. Moreover, it holds promise for future applications with sunlight.

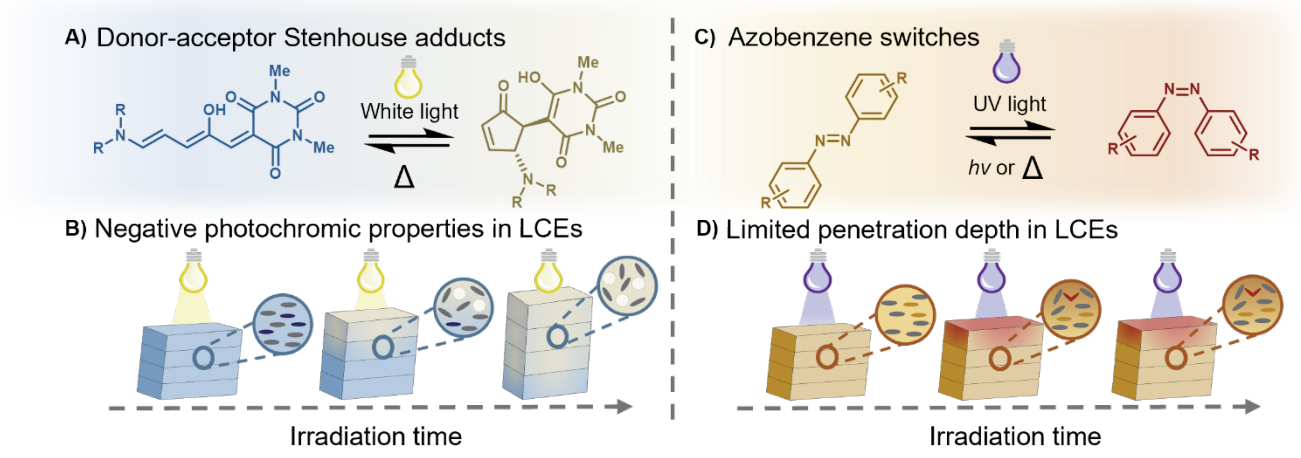

Figure 1. A) Isomerization of DASA photoswitches with broadband light. B) Negative photochromic properties of DASA in a bulk material showing penetration of broadband light. C) Isomerization of azobenzene switches with UV light. D) limited penetration of light cause by azobenzene switches.

2. Results and Discussion

2.1 Film preparation and DASA functionalization

The first objective was to design a thick, aligned LCE-containing conjugated DASA-based photochrome. Due to the incompatibility of DASA molecules with radical intermediates or nucleophilic thiols and amines, we focused on the preparation of polysiloxane-based side-chain LCEs. Finkelmann pioneered the introduction and advancement of an efficient method for incorporating liquid crystal mesogens into polydimethylsixoane (PDMS)-based materials, resulting in the preparation of well-aligned LCEs with thickness up to 500 μm and excellent mechanical performance.[6,57–60] These LCEs are known to have high order parameters (S ~ 0.7), low glass transition temperatures (T_g ~ 0 °C), and moderate nematic-to-isotropic temperatures (T_{ni} ~ 80 °C). This method, commonly referred to as the "Finkelmann method", involves functionalizing polymethylhydrosiloxane (PHMS) with a mesogen and photoresponsive molecule (traditionally azobenzene)[6,57–59,61–63] while forming the crosslinking structure through a time-dependent, two-step platinum-catalyzed hydrosilylation process. We were drawn to this method because it allows for the production of thick, durable, and easy-to-fabricate actuators. Moreover, we hypothesized that a new late-stage functionalization approach could be used to efficiently incorporate DASA-based photochromes without disrupting the thermomechanical properties of the LCEs.[64]

We previously established that the DASA formation reaction between an aromatic amine ("donor" and an activated furan ("acceptor") tends to be a highly efficient,[65] selective,[54,66] and rapid when catalyzed with 1,1,1,3,3,3-hexafluoroisopropanol (HFIP).[67] Although direct incorporation of DASA molecules is not possible due to incompatibility with platinum-catalyzed hydrosilylation chemistry, the DASA-based LCE was prepared by introducing the donor amine in the initial hydrosilylation reaction (**Figure 2A**).[49] A high molecular weight PHMS, mesogens, crosslinker and *N*-(but-3-en-1-yl)-4-methoxyaniline (DASA donor) were dissolved in toluene. This mixture was placed in a spinning Teflon mold and was heated to 70 ºC for 1 h and spun at 8,000 rpm. Afterwards, the mold was cooled to room temperature and the elastomer (not fully cross-linked) was mechanically aligned by stretching to about 1.6 times its original length. In order to fix this uniaxial alignment, the cross-linking reaction was

completed by leaving the sample under load at room temperature for 24 hrs. The cross-linked aligned film was then soaked in toluene (10 mL), followed by dichloromethane (DCM, 10 mL) to remove the platinum catalyst and non-reacted monomers.[49] After removal of the catalyst, the film was added to a solution of the barbituric acid acceptor (5-(furan-2-ylmethylene)-1,3-dimethylpyrimidine-2,4,6(1H,3H,5H)-trione) (DASA acceptor) in dichloromethane with HFIP (20% v/v) and allowed to react overnight (**Figure 2B**). The resulting DASA functionalized film was sequentially washed with dichloromethane (DCM) and then toluene. The substitution of solvents was deemed crucial due to the high evaporation rate of DCM, which results in mechanical fracture of the films during solvent removal. After the solvent switch, the film was de-swelled under vacuum overnight at room temperature, resulting in the desired DASA LCE. Full experimental procedures and characterization are described in the supplementary information.

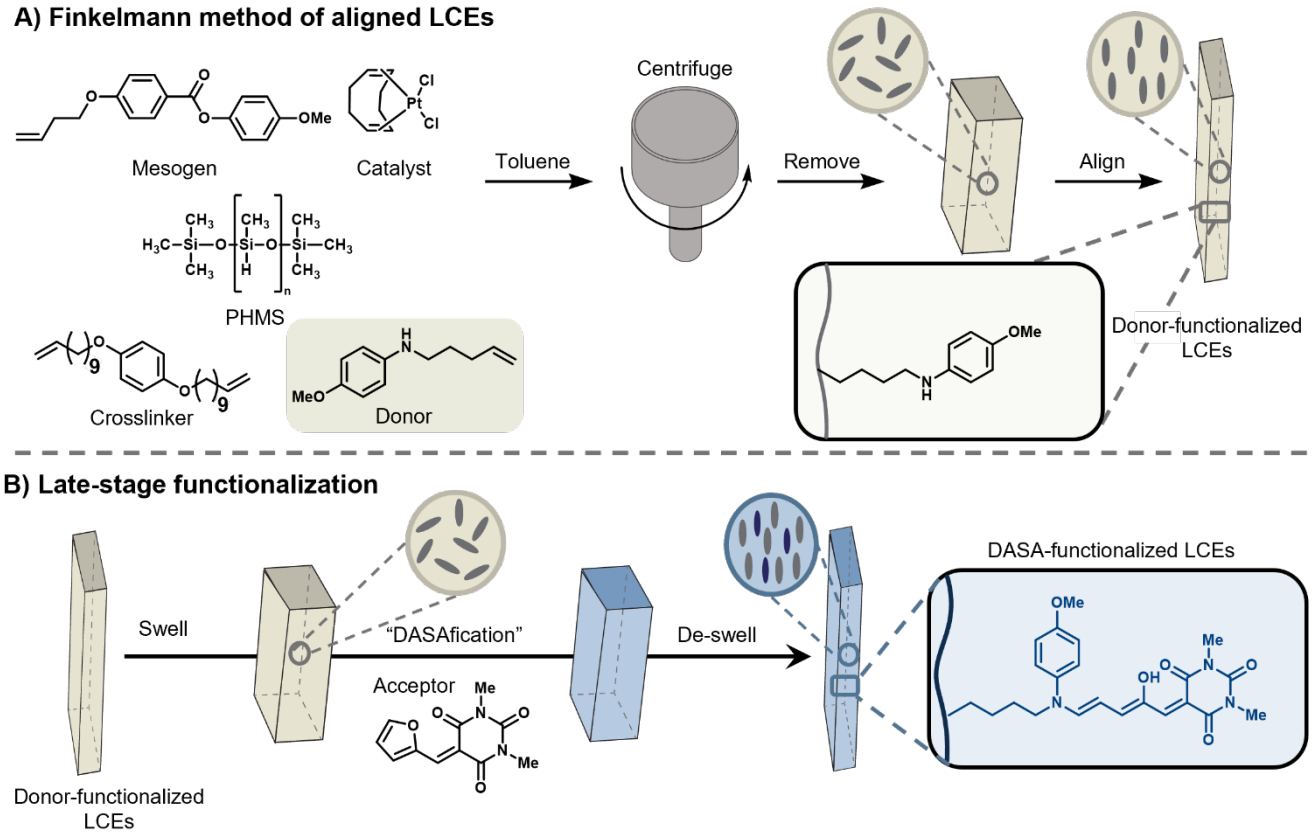

Figure 1. **Fabrication of DASA LCEs** A) Methodology used to obtain aligned polymethylsiloxane LCEs using the original Finkelmann method; B) Late-stage functionalization used to introduce DASA in polymethylsiloxane LCEs. Thickness of the films was determined to be between 360 and 460 μm, measured by a high precision caliper with an accuracy of ± 0.001 mm.

2.2 Effect of DASA in the thermomechanical properties and LC alignment

The effect on the molecular alignment from the late-stage functionalization of the LCE with DASA was assessed with polarized optical microscopy (POM) and 2D-WAXD spectroscopy. For comparison with a non-functionalized LCE film (D-LCE-0), three samples were prepared with varying weight percent (wt.%) of DASA incorporation (0.07 wt.% DASA (D-LCE-1), 0.7 wt.% DASA (D-LCE-2) and 3.5 wt.% DASA (D-LCE-3). Full stoichiometry of monomers used for film fabrication are reported in **Table S1**. Through POM, we observe a difference in brightness for D-LCE-0 when rotating analyzer/polarizer pair from 0º to 45º away from the LCE main axis, indicating the films are crosslinked with a strong uniaxial alignment (**Figure S1**). The POM for D-LCE-1, D-LCE-2 and D-LCE-3 show no significant difference in birefringence. Although unexpected, we attribute this to the high absorbance of DASA. Therefore, we focused on 2-dimentional (2D) wide angle X-ray diffraction (WAXD) to assess the molecular alignment and compare the LCE films. 2D-WAXD data exhibit two distinct diffractions on the equator for all four LCE samples (**Figure 3B**). The order parameter S calculated for all four samples was high, $S > 0.55$. This supports that the late-stage functionalization process is not detrimental to the molecular alignment and is strong evidence that the permanent crosslinks enforce the original molecular order. The order parameter of D-LCE-0, D-LCE-1 and D-LCE-2 are all very similar, $S = 0.71$, $S = 0.69$ and $S = 0.70$, respectively. At the highest loading studied, 3.5 wt.%, a slight decrease of the order parameter is observed (D-LCE-3, $S = 0.56$). Future studies will examine the effects of higher loading and the generality of the late-stage functionalization method.

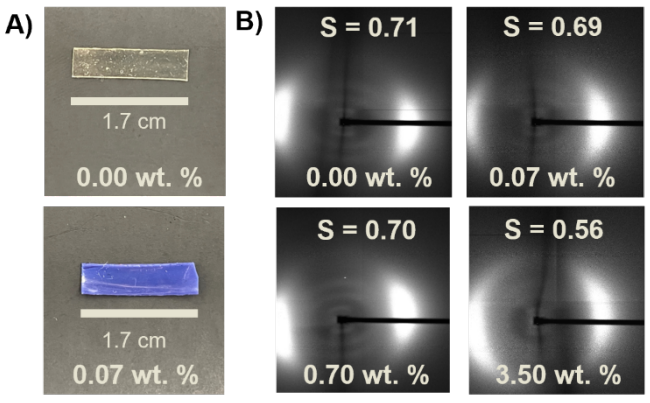

Figure 2. A) Pictures of LCEs prepared using Finkelmann method with 0.00 wt.%, and 0.07 wt.% of DASA (D-LCE-0 and D-LCE-1). B) 2D-Wide angle X-ray Scattering of D-LCE 0, 1, 2 and 3.

2.3 Characterization of DASA LCE

After synthesis of the DASA LCE, the photoresponsive behavior was investigated to determine the relationship between optical properties, light intensity, and material response. To characterize the optical response observed in **Figure 4-AI** (i.e., bleaching of the entire 400 μm D-LCE-1 film with 100 mW cm^{-2} white light), solid state time-dependent UV-Vis spectroscopy was performed. All spectroscopic measurements were conducted with D-LCE-1 because the high molar absorptivity of DASA resulted in transmitted intensities outside the dynamic range of the spectrometer when measuring the absorbance of the more concentrated samples (D-LCE-2 and D-LCE-3) (absorbances >> 4 a.u.). The LCE film was irradiated with a 532 nm light source with a power of 19.9 mW, at room temperature. (**Figure 4-AII**). Of note, a relatively low intensity light was used to help minimize the photothermal effect and avoid change in dimensions during these experiments. Under these conditions, the photostationary state was reached after 700 s and no red-shifted shoulder corresponding to an intermediary state were observed (**Figure S2**). **Figure 4-AIII** shows excellent reversibility after ten cycles, cycling between irradiation with 532 nm light (30 s) and recovery in the dark (12 min).

The molecular alignment of DASA within the LCE network was measured by polarized UV-Vis spectroscopy. **Figure 4-AIV** shows the angular dependance of the polarized absorption of D-LCE-1, with the stretching direction serving as the molecular frame of reference (perpendicular). When the sample is positioned at 90° degrees from the linear polarizer, an absorbance of 1.8 a.u. was measured. An increase to 2.8 a.u. is observed when the sample is set at 0° from the polarizer. From these measurements, the linear dichroism (*D*) at 532 nm was calculated using the following equation $D = \frac{A_{\perp} - A_{\parallel}}{A_{\perp} + 2A_{\parallel}}$ and determined to be -0.18. This indicates that the linear open configuration of DASA is oriented in the LC direction and supports the 2D-WAXD data showing alignment of photochromic functionalized LCE films. Furthermore, it suggests promising prospects for future applications of this late-stage functionalization process in angle-dependent photoisomerization kinetics and photochemically driven LCEs.

To further investigate effects of DASA loading on the mechanical properties of the material, differential scanning calorimetry (DSC) was performed. As discussed, 2D-WAXD for all four samples showed excellent alignment and were consistently high (S > 0.55). Therefore, we hypothesized that changes to the weight percent of DASA incorporated into the LCE would follow the same trend and have a minimal effect on T_g and T_{ni}. As shown in **Figure 4-BV**, as the DASA loading increased and the percent of mesogen monomer decreased, the nematic-to-isotropic temperature decreased linearly from 78 °C to

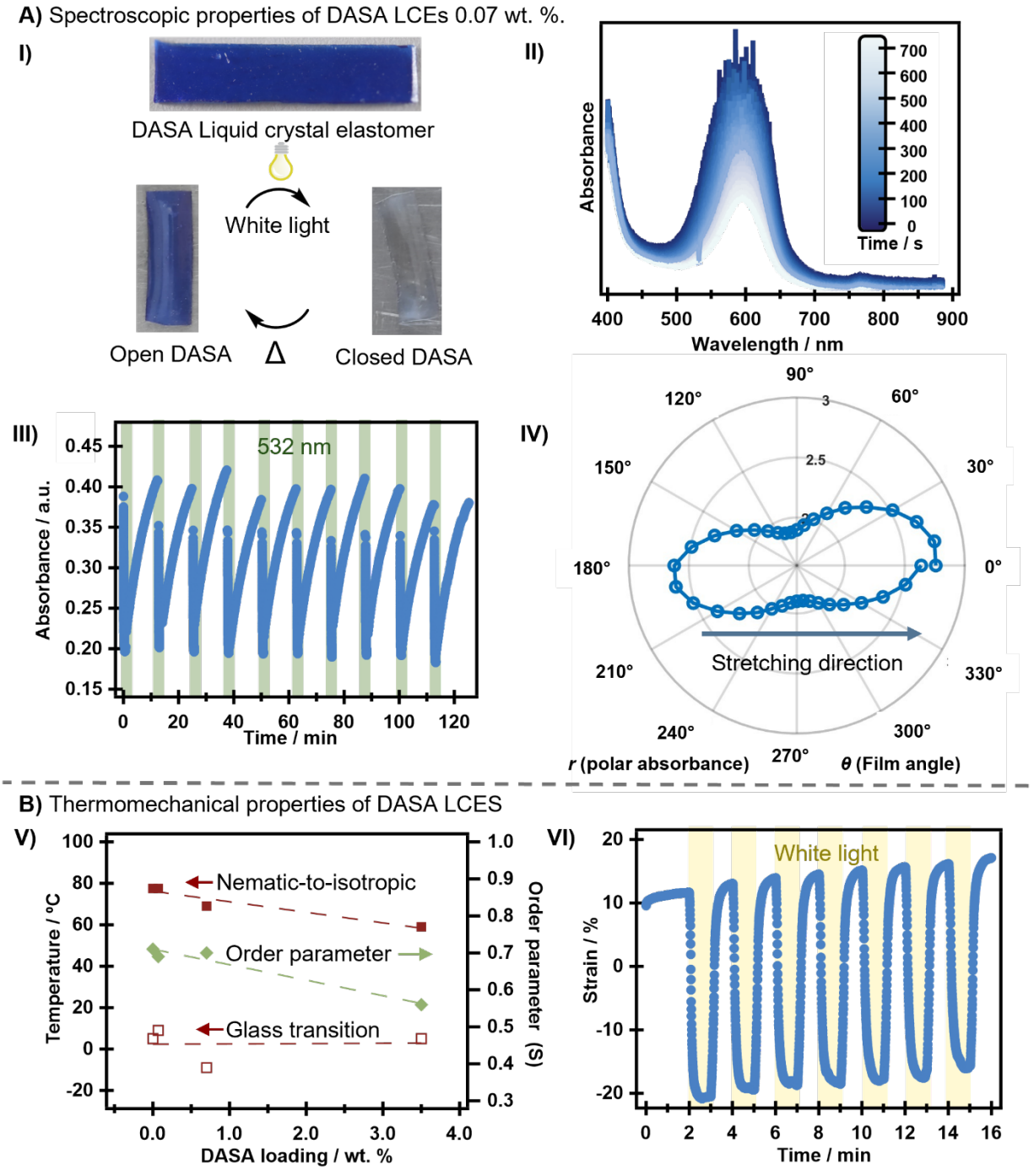

Figure 4. A) I. Pictures of DASA LCE in its open and in its closed form. II. Spectrum and bleaching when irradiated with 532 nm light over 700s. Small fluctuation of absorbance at 532 nm corresponds to the scattered light from the 532 nm laser used to pump the sample. III. Switching cycles of DASA LCE when irradiated with 532 nm light. IV. Polarized absorbance of DASA LCE measured at 532 nm. B) V. Plot of the glass transition and nematic-to-isotropic temperature and order parameter as a function of DASA loading in the LCE. VI. Actuation cycles of DASA LCE when irradiated with white light at constant stress.

60 °C. This behavior is consistent with the linear decrease in order parameter determined by 2D-WAXD. Interestingly, the glass transition temperature remains almost constant throughout the series of DASA-functionalized LCE examined. This is in contrast to results we previously observed with higher T_g DASA-polymer conjugates;[68] however, we caution drawing direct comparisons between these two very different polymer materials. Following these results, thermomechanical analysis of the D-LCE-1 films was conducted using a dynamic mechanical analyzer (DMA). At a constant force of 0.0005 N, the film contracted ~20% in the nematic direction upon white light irradiation with a power of 300 mW cm^{-2}. Notably, this equals the full contractions observed in **Figure S3** (20% strain) as the sample was heated thermally to T_{ni} in the DMA. Additionally, **Figure 4-BVI** shows that the material can undergo seven cycles within a 20 min period with minimal change in peak strain or recovery. Maximum strain contraction is achieved within 30 s of irradiation, and once the irradiation is halted, the film returns to its original length after another 30 s. This validates that using a low concentration (0.07 wt%) of DASA photoswitch enables efficient actuation behavior in the thick LCE films using readily available white light irradiation.

2.4 2D (Planar) actuation properties of the DASA-LCEs

Based on contraction studies under load in the DMA, we next sought to study the actuation response of the DASA LCE using a free-standing film. So far, most photo-driven systems with thick LCEs films have taken advantage of out-of-plane bending actuation controlled by photothermal effects. If heat disperses less rapidly throughout the entire thickness of the film compared to cooling effects to the surrounding environment, a temperature gradient will form within the film.[28] This thermal gradient results in bending when the film temperature increases above T_{ni}. As such, reducing the thermal gradient,

through efficient light penetration across the entire sample or through heat dissipation, should enable 2D contraction and elongation actuation (planar, no bending).[17] To test these properties, a 0.5 cm × 0.7 cm × 400 μm film with 0.07% DASA was placed on a flat surface and irradiated with white light (power = 200 mW cm^{-2}) located approximately 2 cm from the film. An initial small bending of the film is observed, followed by a large planar contraction and complete bleaching (**Figure 5 I-IV**). Interestingly, the film remains contracted and appears transparent if the light irradiation is maintained (**Figure 5V**). We attribute this behavior to an equilibrium between the open and closed form of DASA, which helps maintain a constant temperature above T_{ni} under these irradiation conditions (*vide infra*). When irradiation is stopped, the color returns back almost immediately, and the film returns to its original elongated shape after 5 s. **Figure S4** shows that this planar 2D type of actuation is reversible and can go through several cycles. To further highlight the ability to penetrate light throughout the bulk of the D-LCE films, we sought to irradiate the LCE film through the 400 μm edge of the film that is 0.5 cm in length. Two sets of glass slides were placed on top and bottom of the D-LCE-1 film, helping to guide the light. Efficient activation of the DASA-active layer was achieved, evidenced by bleaching (**Figure S5**). These results reveal that activation of the D-LCE can be achieved by irradiation from all sides of the film because the light penetration depth is on the millimeter to centimeter length scale. This presents new opportunities to expand beyond irradiating LCE films solely in the orthogonal plane and potentially achieve photoactuation in bulk 3-D structures.

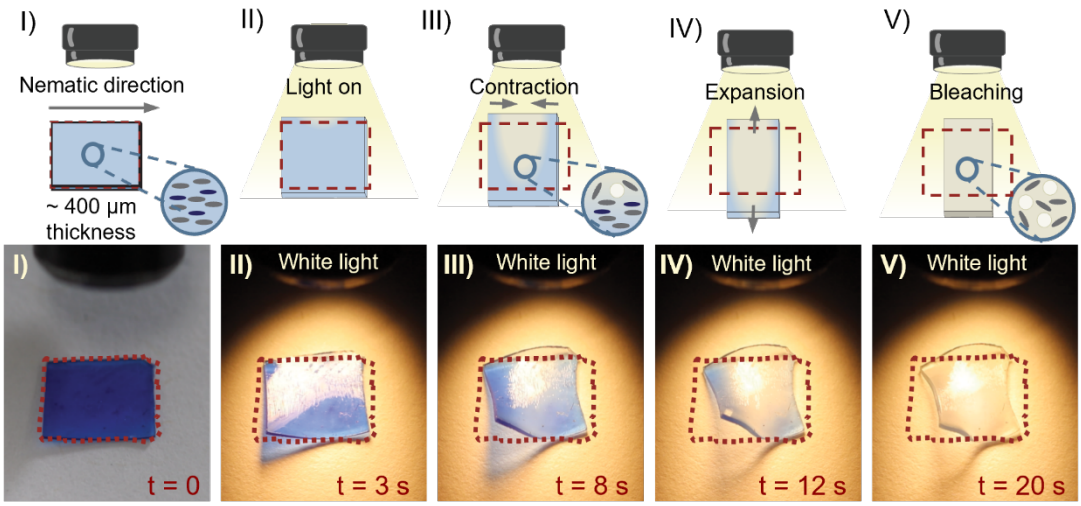

Figure 5. Schemes and pictures showing full bleaching and contraction of D-LCE-1 throughout the 400 µm of thickness of the material. Simultaneous bleaching and contraction of the film is observed in the first cycle **Video S1**.

The free-standing films (2 cm x 0.5 cm x 400µm) were then vertically fixed, to explore the photoresponsive behavior under a traditional bending configuration. Compared to the above studies, a slightly higher intensity of white light irradiation (300 mW cm^{-2}) was used. As shown in **Figure S6** and **Video S2**, the film initially bends towards the light and then contracts along the director. As shown in **Figure S7**, the sample starts bending almost immediately upon light irradiation, researching a maximum bending angle after 10 s. The whole sample contracts along the director as irradiation continues. The temperature change caused by illumination was measured using an IR camera. During the first 10 s (bending is predominantly observed), the temperature increases to 45 ºC which is below T_{ni}. After 25 s of irradiation, the temperature transitions above T_{ni} to a maximum temperature of 75 ºC. Photothermal heating is to be expected due to the high molar absorptivity of DASA-based photochromes; however, we were surprised to find the films remaining highly colored during illumination (i.e., no bleaching observed). As a result, a constant temperature is maintained when the light is on, analogous to traditional photothermal agents. We attribute this behavior to a fraction of the population of DASA remaining in the open form, which is capable of absorbing light and generating photothermal heat. When the light irradiation is stopped, the sample cools down in a matter of seconds and the film returns to its original

state. A full detailed study uncovering the photothermal and photochemical contributions to the light-responsive actuation within this system will be explored in a follow up study.

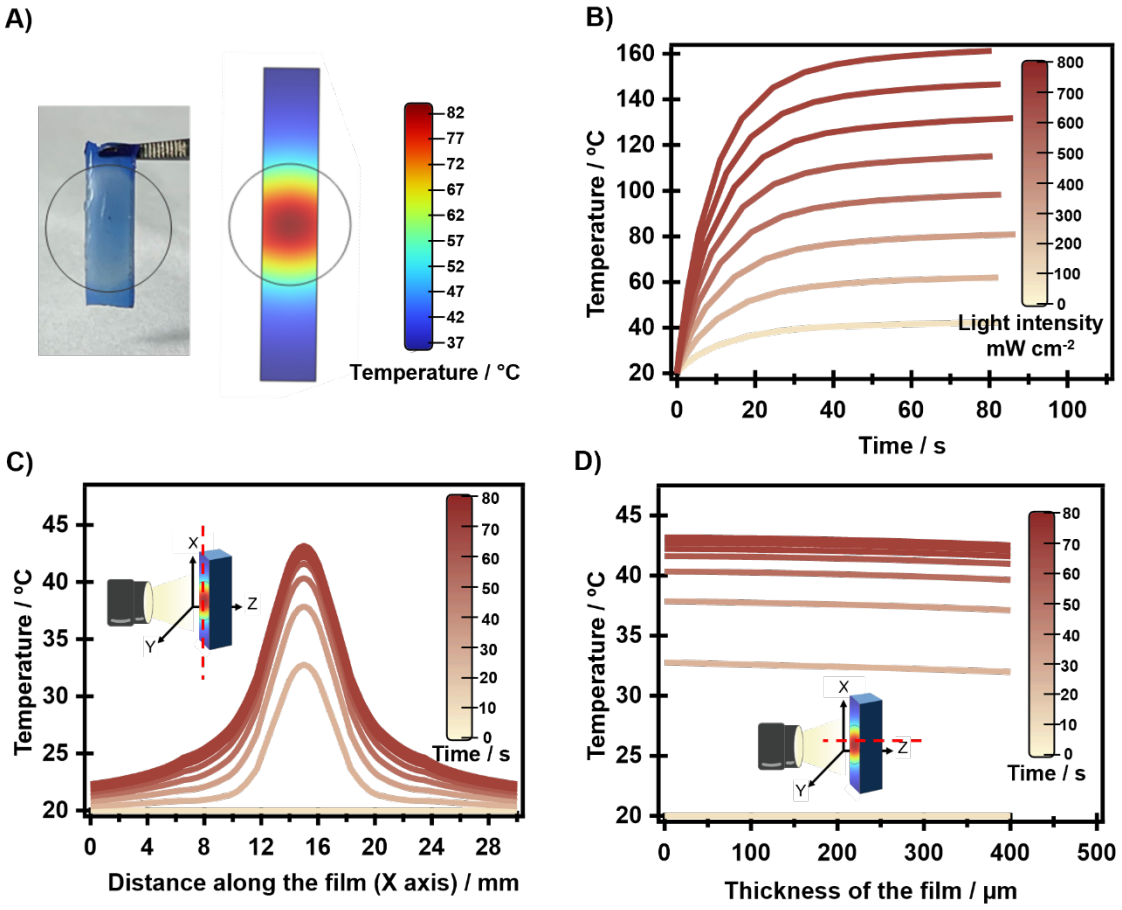

Figure 6 . A) Pictures of D-LCE-1 showing regions of high intensity at the center of the film compared to the COMSOL simulations of the photothermal effect. B) Simulations of maximum temperature reached as a function of light intensity and time. C) Simulations of the temperature profile along the length of D-LCE-1. D) Simulations of the temperature profile of the D-LCE-1 across the thickness of the film as a function of time.

During our studies exploring the reactivity of free-standing films, we made an interesting observation that suggests a relationship between light intensity and the open and closed form equilibrium of DASA. As shown in **Figure 6A**, the regions of the film exposed to higher light intensity (at the center of the irradiation spot) retained a deeper blue coloration, contrasting with the less saturated areas towards the boundary of the exposed region. We hypothesized that this effect stemmed from photothermal heating that shifted the equilibrium between the open and closed form of DASA, even under constant light irradiation. To test this, we monitored the reaction as a function of temperature under constant irradiation. D-LCE-1 was bleached with low intensity light (100 mW cm^{-2}) and then placed on a heating plate set to

25 ºC. Under constant irradiation with 100 mW cm^{-2} power the film was slowly heated to 80 ºC. As the temperature increased, the sample became visually more colored (**Figure S8**). These results illustrate how the temperature increase initiates a feedback loop, which drives the DASA equilibrium to its original highly colored state and consequently helps maintain a constant temperature throughout the material. To further understand role of photothermal heating, the LCE film heating was simulated with COMSOL Multiphysics Heat Transfer in Solids and Fluids Module. The heating induced by light irradiation was modeled within a circular domain in the center of the film, and the rate of heat generation within the material was derived from the incident light flux and the sample absorbance, assuming perfect photothermal efficiency and using the Beer-Lambert law to model absorbance. As shown in **Figure 6B**, at 300 mW cm^{-2} and 100 mW cm^{-2}, the increase in temperature of the simulations is consistent with temperatures recorded experimentally of 40 °C and 80 °C, respectively (**Figure S9 and Figure S10**). The Gaussian behavior of the temperature along the length of the film is plotted in **Figure 6C**, as a function of time from 0 to 80 s. The temperature profile of the film can also be modeled throughout the thickness of the film. Here, no thermal gradient was observed in D-LCE-1 when irradiated with 100 mW cm^{-2} light in air (**Figure 6D**), which is consistent with minimal bending being observed experimentally under these conditions (**Figure S11**).[31] While the underlying actuation mechanism with high-intensity light implies a photothermal process, the observed photo-bleaching with lower intensities of light suggests that regulating heat dissipation and light intensity is crucial for controlling light penetration depth. In turn, this may also help to distinguish between photochemical and photothermal driven actuation.

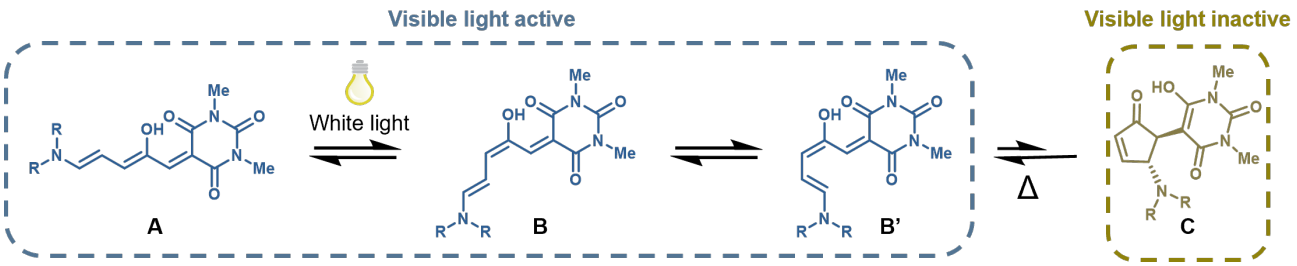

Figure 7. Simplified diagram illustrating DASA photoisomerization mechanism, highlighting light responsive and non-light responsive intermediates.

These results align with the isomerization mechanism of DASA: When exposed to visible light, DASA photochromes undergo a rapid actinic step on the picosecond time scale, forming photoisomer B

(**Figure 7**). The actinic step is followed by a series of slower steps that can proceed thermally along the multistep reaction pathway – bond rotation B → B' and 4π electrocyclization B' → C. For efficient formation of the closed isomer under irradiation, the forward direction steps need to be fast and outcompete the thermal back reaction C → B'. The equilibrium between the forward photoreaction and the thermal back reaction is temperature dependent and will reach a photothermal stationary state (PTSS) at equilibrium. At higher light intensity, the photothermal heat becomes sufficiently high to drive the metastable closed form of DASA back to the highly colored form (i.e., shifting the PTSS equilibrium to the open form). Although it is known that the PTSS for DASA is governed in part by the thermal back reaction, to our knowledge, using the *in situ* generated photothermal heat as a feedback loop to tune the bleaching front in solid-state materials has not been explored.[50]

2.5 Controlling the Light Penetration Depth in Large 3D Structures.

Based on the above results, we next investigated a larger three-dimensional (3D) structure by layering fourteen 400 μm D-LCE-1 thick films on top of each other to create a sample with dimensions 0.5 cm width, 0.7 cm in length and over 0.5 cm in height. As seen in **Figure 8**, irradiation with 300 mW cm^{-2} light results in contraction along the nematic direction and expansion in the vertical direction, as expected (**Figure 8A I-III**). As light irradiation continues, the temperature also increases due to the photothermal heating from the highly absorbing open form of DASA. This creates a feedback loop that shifts the DASA equilibrium back to the original highly colored state and further increases the temperature of the material (**Figure 8A IV)**. After ~100 s the material reaches a PTSS and the temperature increases above T_{ni}, resulting in complete contraction of the 3D structure **Figure 8A V**.

To enable full bleaching of the fourteen-layer stack, the sample was placed underwater to provide a reservoir for dissipating the photothermal heat. This minimizes the thermally driven back reaction of DASA that generates the colored form and facilitate better light penetration. Under these conditions, we observed full bleaching of the stacked 3D structure within 70 s of light irradiation, (**Figure 8B I-IV**). As expected, contraction along the nematic direction and expansion in the orthogonal plane were observed, albeit substantially less than observed in air. When the light is turned off, the structure returns almost

immediately to its original size and the color returns to all fourteen-layers after 15 min (**Figure 8B V and Figure S12**). Presumably, increasing the DASA loading or incorporating it into the backbone of the LCE would further improve the magnitude of the photochemical actuation underwater. Nevertheless, light penetration is observed throughout the bulk of the 0.55 cm sample, which represents almost four orders of magnitude greater than traditional azobenzene-based LCEs (from a few microns to a few millimeters).

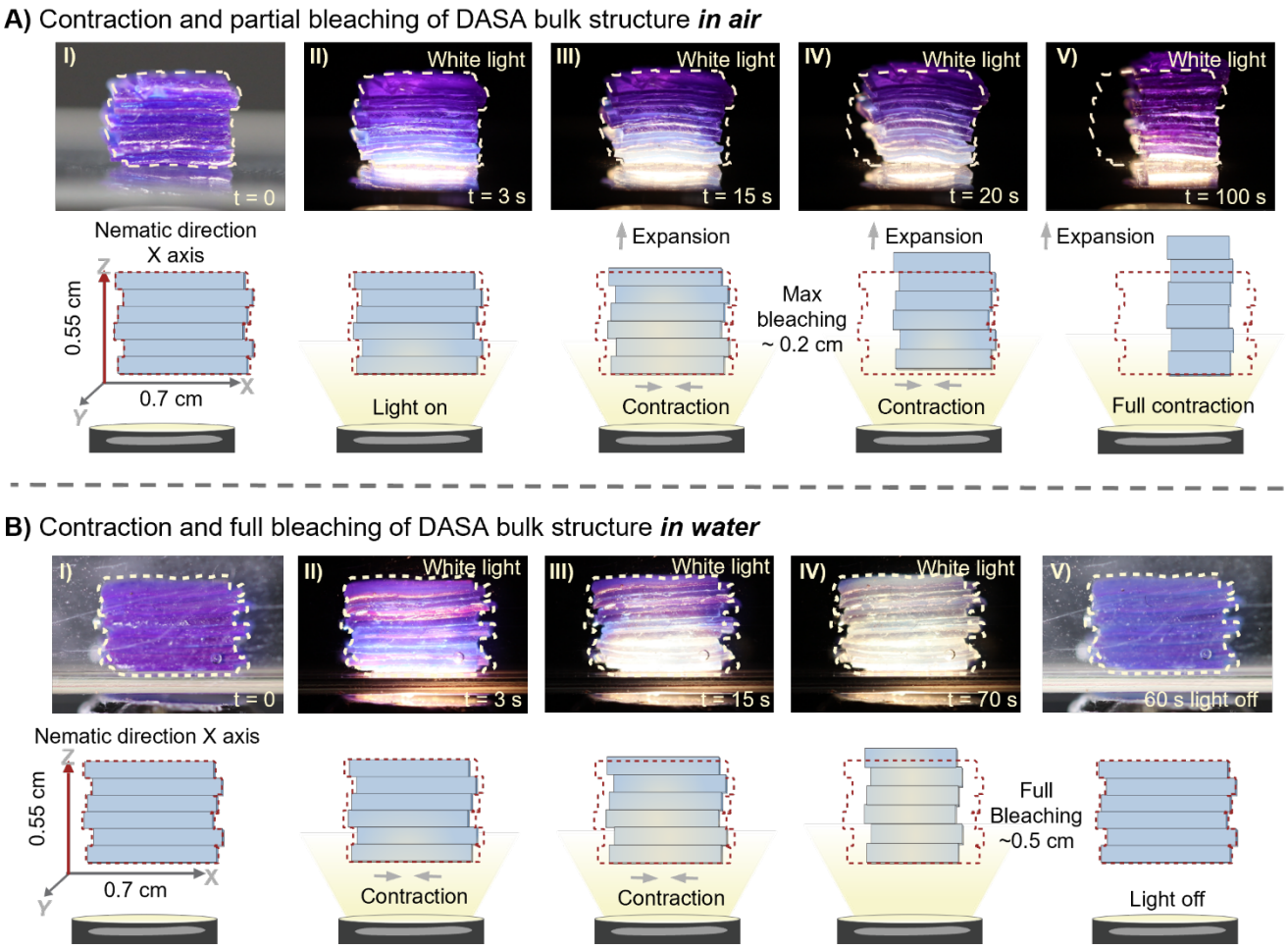

Figure 8. Contraction and bleaching of a 3D structure (cube) measuring 0.55 cm in height, 0.7 cm in length and 0.5 cm in width using white light A) in air and B) underwater. **Video S3 and Video S4**.

2.6 Conclusion

In this report, we described the synthesis and application of a late-stage functionalization strategy to prepare a novel LCE platform that enables the use of broadband visible (white) light. This strategy provides access to well-aligned, thick (400 µm to 5 mm) polysiloxane-based LCEs functionalized with donor-acceptor Stenhouse adduct (DASA) side-chains. The effects on the molecular alignment from the late-stage functionalization with DASA of the new materials were studied using three different DASA-

LCE with varying weight percent (wt.%) of DASA incorporation. All three samples form well-aligned LCE networks, order parameter ranging between S = 0.55 and 0.71, with excellent mechanical properties. This study provides strong evidence that the late-stage functionalization process is not detrimental to the molecular alignment observed in the traditional Finkelmann method. We demonstrate the ability of large films (0.5 cm × 0.7 cm × 400 μm) with only 0.07% DASA to undergo 2D planar actuation and full bleaching upon irradiation with low intensity visible light, a process that is repeatable over several cycles. We showed the influence of light intensity and subsequent heat generation on the photothermal stationary state equilibrium of DASA. Through careful control of the light intensity and heat dissipation, we highlight the ability to fully bleach a fourteen-layer stacked LCE system with a thickness of 0.55 cm. This work illustrates the importance of expanding the photochromic material incorporated into LCE-based actuators and provides the foundation to move beyond thin film, UV-light based systems. We anticipate that thick, durable, and easy-to-fabricate visible-light activated DASA-LCEs will promote their use, and their continued development will be used to unlock future applications at the interface of soft robotics and living beings.

Acknowledgements

We thank Dr. Peter Palffy-Muhoray and Dr. Mykhailo Pevnyi for their assistance in constructing the Teflon mold utilized in the Finkelmann method and for providing guidance on film preparation techniques. We also thank Dr. Friedrich Stricker, Dr. Michelle Clerc, Dr. Julie Peterson, Dr. Andrei Nikolaev, and Dr. Sophia Bailey for helpful suggestions during the development of this project. This research reported here was supported by the Office of Naval Research through the MURI on Photomechanical Materials Systems (ONR N00014-18-1-2624). The authors acknowledge the National Science Foundation (NSF) (grant no. MRI-1920299) for the acquisition of Bruker 500 MHz and 400 MHz NMR instruments. MP was partially supported by Basic Science Research Program through the National Research Foundation of Korea (NRF) funded by the Ministry of Education (grant no. 2020R1 A6 A3 A03037524).

Received: ((will be filled in by the editorial staff))
Revised: ((will be filled in by the editorial staff))
Published online: ((will be filled in by the editorial staff))

4. References

[1] K. M. Herbert, H. E. Fowler, J. M. McCracken, K. R. Schlafmann, J. A. Koch, T. J. White, *Nat. Rev. Mater.* **2022**, *7*, 23–38.
[2] M. Warner, E. M. Terentjev, *Liquid Crystal Elastomers*, Oxford University PressOxford, **2003**.
[3] C. Ohm, M. Brehmer, R. Zentel, *Adv. Mater.* **2010**, *22*, 3366–3387.
[4] T. J. White, D. J. Broer, *Nat. Mater.* **2015**, *14*, 1087–1098.
[5] S. W. Ula, N. A. Traugutt, R. H. Volpe, R. R. Patel, K. Yu, C. M. Yakacki, *Liq. Cryst. Rev.* **2018**, *6*, 78–107.
[6] J. Kiipfec, H. Finkelrnann. *Makromol. Chem. Rapid Commun*. **1991**, *726*, 717–726.
[7] D. J. Broer, I. Heynderickx, *Macromol.*, **1990**, *23*, 2474-2477.
[8] A. Kotikian, R. L. Truby, J. W. Boley, T. J. White, J. A. Lewis, *Adv. Mater.* **2018**, *30*, 1706164.
[9] S. Li, G. Librandi, Y. Yao, A. J. Richard, A. Schneider-Yamamura, J. Aizenberg, K. Bertoldi, *Adv. Mater.* **2021**, *33*, 2105024.
[10] K. Fukuhara, S. Nagano, M. Hara, T. Seki, *Nat. Commun.* **2014**, *5*, 3320.
[11] M. Lahikainen, H. Zeng, A. Priimagi, *Nat. Commun.* **2018**, *9*, 4148.
[12] Z. Hu, Y. Li, T. Zhao, J. an Lv, *Appl. Mater. Today.* **2022**, *27*, 2352-9407.
[13] T. Zhao, W. Fang, Y. Fan, Z. Hu, H. Wu, X. Q. Feng, J. an Lv, *Adv. Mater. Technol.* **2022**, 2101660.
[14] H. Shahsavan, A. Aghakhani, H. Zeng, Y. Guo, Z. S. Davidson, A. Priimagi, M. Sitti, *Proc. Natl. Acad. Sci. U. S. A.* **2020**, *117*, 5125–5133.
[15] J. A. Lv, Y. Liu, J. Wei, E. Chen, L. Qin, Y. Yu, *Nature.* **2016**, *537*, 179–184.
[16] Y. Hong, A. Buguin, J. M. Taulemesse, K. Kaneko, S. Méry, A. Bergeret, P. Keller, *J. Am. Chem. Soc.* **2009**, *131*, 15000–15004.
[17] L. B. Braun, T. Hessberger, R. Zentel, *J. Mater. Chem. C. Mater.* **2016**, *4*, 8670–8678.
[18] C. L. Van Oosten, K. D. Harris, C. W. M. Bastiaansen, D. J. Broer, *Eur. Phys. J. E.* **2007**, *23*, 329–336.
[19] H. Zeng, H. Zhang, O. Ikkala, A. Priimagi, *Matter.* **2020**, *2*, 194–206.
[20] H. Zeng, O. M. Wani, P. Wasylczyk, R. Kaczmarek, A. Priimagi, *Adv. Mater.* **2017**, *29*, 1701814.
[21] S. Li, M. M. Lerch, J. T. Waters, B. Deng, R. S. Martens, Y. Yao, D. Y. Kim, K. Bertoldi, A. Grinthal, A. C. Balazs, J. Aizenberg, *Nature.* **2022**, *605*, 76–83.
[22] O. M. Wani, R. Verpaalen, H. Zeng, A. Priimagi, A. P. H. J. Schenning, *Adv. Mater.* **2019**, *31*, 1805985.
[23] S. Serak, N. Tabiryan, R. Vergara, T. J. White, R. A. Vaia, T. J. Bunning, *Soft Matter.* **2010**, *6*, 779–783.
[24] H. Yu, T. Ikeda, *Adv. Mater.* **2011**, *23*, 2149–2180.
[25] H. K. Bisoyi, A. M. Urbas, Q. Li, *Adv. Opt. Mater.* **2018**, *6*, 1800458.
[26] N. P. Skillin, G. E. Bauman, B. E. Kirkpatrick, J. M. McCracken, K. Park, R. A. Vaia, K. S. Anseth, T. J. White, *Adv. Mater.* **2024**, 2313745.
[27] A. S. Kuenstler, Y. Chen, P. Bui, H. Kim, A. DeSimone, L. Jin, R. C. Hayward, *Adv. Mater.* **2020**, *32*, 2000609.
[28] Y. Wang, A. Dang, Z. Zhang, R. Yin, Y. Gao, L. Feng, S. Yang, *Adv. Mater.* **2020**, *32*, 2004270.
[29] H. Kim, J. A. Lee, C. P. Ambulo, H. B. Lee, S. H. Kim, V. V. Naik, C. S. Haines, A. E. Aliev, R. Ovalle-Robles, R. H. Baughman, T. H. Ware, *Adv. Funct. Mater.* **2019**, *29*, 1905063.
[30] J. E. Marshall, E. M. Terentjev, *Soft Matter.* **2013**, *9*, 8547–8551.
[31] B. Zuo, M. Wang, B. P. Lin, H. Yang, *Nat. Commun.* **2019**, *10*, 4539.
[32] O. S. Bushuyev, M. Aizawa, A. Shishido, C. J. Barrett, *Macromol. Rapid. Commun.* **2018**, *39*, 1700253.
[33] Z. Zhang, W. Wang, M. O'Hagan, J. Dai, J. Zhang, H. Tian, *Angew. Chem. Int. Ed.* **2022**, *61*, 2205758.

[34] M. Gao, D. Kwaria, Y. Norikane, Y. Yue, *Nat. Sci.* **2023**, *3*, 220020.
[35] R. Yin, W. Xu, M. Kondo, C. C. Yen, J. I. Mamiya, T. Ikeda, Y. Yu, *J. Mater. Chem.* **2009**, *19*, 3141–3143.
[36] T. Ikeda, M. Nakano, Y. Yu, O. Tsutsumi, A. Kanazawa, *Adv. Mater.* **2003**, *15*, 201–205.
[37] K. M. Lee, M. L. Smith, H. Koerner, N. Tabiryan, R. A. Vaia, T. J. Bunning, T. J. White, *Adv. Funct. Mater.* **2011**, *21*, 2913–2918.
[38] K. Min Lee, B. M. Lynch, P. Luchette, T. J. White, *J. Polym. Sci. A. Polym. Chem.* **2014**, *52*, 876–882.
[39] S. Iamsaard, E. Anger, S. J. Aßhoff, A. Depauw, S. P. Fletcher, N. Katsonis, *Angew. Chem.* **2016**, *128*, 10062–10066.
[40] D. Ditter, L. B. Braun, R. Zentel, *Macromol. Chem. Phys*. **2020**, *221*, *1900265*.
[41] K. Kumar, C. Knie, D. Bléger, M. A. Peletier, H. Friedrich, S. Hecht, D. J. Broer, M. G. Debije, A. P. H. J. Schenning, *Nat. Commun.* **2016**, *7*, 11975.
[42] S. Fredrich, T. Engels, A. P. H. J. Schenning, *ACS. Appl. Polym. Mater.* **2022**, *4*, 7751–7758.
[43] W. Wu, L. Yao, T. Yang, R. Yin, F. Li, Y. Yu, *J. Am. Chem. Soc.* **2011**, *133*, 15810–15813.
[44] Z. Jiang, M. Xu, F. Li, Y. Yu, *J. Am. Chem. Soc.* **2013**, *135*, 16446–16453.
[45] A. Ryabchun, Q. Li, F. Lancia, I. Aprahamian, N. Katsonis, *J. Am. Chem. Soc.* **2019**, *141*, 1196–1200.
[46] M. Lahikainen, K. Kuntze, H. Zeng, S. Helantera, S. Hecht, A. Priimagi, *ACS. Appl. Mater. Interfaces.* **2020**, *12*, 47939–47947.
[47] T. S. Hebner, M. Podgórski, S. Mavila, T. J. White, C. N. Bowman, *Angew. Chem. Int. Ed.* **2022**, *61*, 2116522.
[48] H. Nie, J. L. Self, A. S. Kuenstler, R. C. Hayward, J. Read de Alaniz, *Adv. Opt. Mater.* **2019**, *7*, 1900224.
[49] M. Clerc, C. Tekin, S. Ulrich, R. V. M. Freire, S. Salentinig, N. Bruns, L. F. Boesel, *Macromol. Rapid. Commun.* **2022**, 2200120.
[50] M. Clerc, S. Sandlass, O. Rifaie-Graham, J. A. Peterson, N. Bruns, J. Read de Alaniz, L. F. Boesel, *Chem. Soc. Rev.* **2023**,*52*, 8245-8294.
[51] S. Helmy, F. A. Leibfarth, S. Oh, J. E. Poelma, C. J. Hawker, J. R. de Alaniz, *J. Am. Chem. Soc.* **2014**, *136*, 8169–8172.
[52] J. R. Hemmer, Z. A. Page, K. D. Clark, F. Stricker, N. D. Dolinski, C. J. Hawker, J. Read de Alaniz, *J. Am. Chem. Soc.* **2018**, *140*, 10425–10429.
[53] J. R. Hemmer, S. O. Poelma, N. Treat, Z. A. Page, N. D. Dolinski, Y. J. Diaz, W. Tomlinson, K. D. Clark, J. P. Hooper, C. Hawker, J. Read de Alaniz, *J. Am. Chem. Soc.* **2016**, *138*, 13960–13966.
[54] F. Stricker, D. M. Sanchez, U. Raucci, N. D. Dolinski, M. S. Zayas, J. Meisner, C. J. Hawker, T. J. Martínez, J. Read de Alaniz, *Nat. Chem.* **2022**, *14*, 942–948.
[55] S. Sandlass, F. Stricker, D. Fragoso, J. Read de Alaniz, M. J. Gordon, *J. Photochem. Photobiol. A. Chem.* **2023**, *444*, 114964.
[56] J. Boelke, S. Hecht, *Adv. Opt. Mater.* **2019**, *7*, 1900404.
[57] J. Schatzle, W. Kaufhold, H. Finkelmam. *Makromol. Chem*. **1989**, *190*, 3269–3284.
[58] H. Finkelmann, H.-J. Kock, G. Rehage, *Makromol. Chem., Rapid. Commun.* **1981**, *2*, 317–322.
[59] G. H. F. Bergmann, H. Finkelmann, V. Percec, M. Zhao, *Macromol. Rapid. Commun.* **1997**, *18*, 353–360.
[60] J. Garcia-Amorós, H. Finkelmann, D. Velasco, *J. Mater. Chem.* **2011**, *21*, 1094–1101.
[61] X. Coqueret, H. Finkelmann, H. J. Kock, G. Rehage, *Macromol. Rapid. Commun.* **2005**, *26*, 665–672.
[62] H. Finkelmann, E. Nishikawa, G. G. Pereira, M. Warner, *Phys. Rev. Lett.* **2001**, *87*, 015501/1-015501/4.
[63] H. Finkelmann, S. T. Kim, A. Muaeoz, P. Palffy-Muhoray, B. Taheri, *Adv. Mater.* **2001,** *13*, 1069-1072.
[64] M. Camacho-Lopez, H. Finkelmann, P. Palffy-Muhoray, M. Shelley, *Nat. Mater.* **2004**, *3*, 307–310.
[65] J. A. Peterson, F. Stricker, J. Read de Alaniz, *Chem. Commun.* **2022**, *58*, 2303–2306.
[66] F. Stricker, J. Peterson, S. K. Sandlass, A. de Tagyos, M. Sroda, S. Seshadri, M. J. Gordon, J. Read de Alaniz, *Chem.* **2023**, *9*, 1994-2005.
[67] M. Clerc, F. Stricker, S. Ulrich, M. Sroda, N. Bruns, L. F. Boesel, J. Read de Alaniz, *Angew. Chem. Int. Ed.* **2021**, *60*, 10219–10227.

[68] J. Lee, M. M. Sroda, Y. Kwon, S. El-Arid, S. Seshadri, L. F. Gockowski, E. W. Hawkes, M. T. Valentine, J. Read De Alaniz, *ACS. Appl. Mater. Interfaces.* **2020**, *12*, 54075–54082.

ToC figure

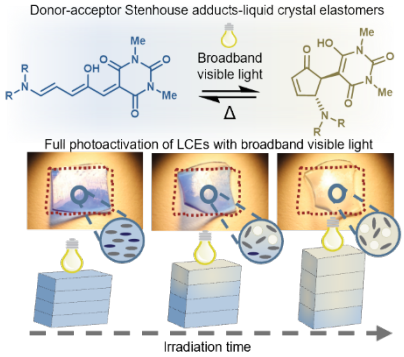

This report presents the synthesis and characterization of DASA-side-chain liquid crystal elastomers (LCEs). Utilizing widely accessible broadband visible light and harnessing the negative photochromic properties of DASA-based photoswitch, we achieve light penetration throughout the LCE structures, reaching thicknesses of up to 5.5 mm.